ELSEVIER

Journal of Alloys and Compounds 450 (2008) 136–141

Journal of ALLOYS AND COMPOUNDS

www.elsevier.com/locate/jallcom

Lattice effect on the magnetic and magneto-transport properties of $(La_{1/3}Sm_{2/3})_{0.67}Ba_{0.33-x}Sr_xMnO_3$ ($x = 0.0$, 0.1, 0.2 and 0.33) compounds

Saket Asthana [a], A.K. Nigam [b], S.K. Malik [b], D. Bahadur [a,*]

[a] *Department of Metallurgical Engineering and Materials Science, Indian Institute of Technology Bombay, Powai, Mumbai 400076, India*
[b] *Tata Institute of Fundamental Research, Colaba, Mumbai 400005, India*

Received 18 May 2006; received in revised form 14 October 2006; accepted 17 October 2006
Available online 20 November 2006

Abstract

The effect of substituting Sr for Ba on the magneto-transport and magnetic properties of $(La_{1/3}Sm_{2/3})_{0.67}Ba_{0.33}MnO_3$ system, has been investigated. The samples, $(La_{1/3}Sm_{2/3})_{0.67}Ba_{0.33-x}Sr_xMnO_3$ ($x = 0.0$, 0.1, 0.2 and 0.33), synthesized by citrate gel route, crystallize in an orthorhombic structure (space group *Pnma*, no. 62). The unit cell volume decreases while the metal-insulator transition temperature (T_{MI}) increases with increasing Sr content. The localization of charge carriers occurs at low temperatures and becomes more pronounced with decreasing Sr content which leads to an enhancement of resistivity. This could be understood by the variation of Mn–O–Mn bond-distance and angle. Reappearance of semiconducting behavior ($d\rho/dT < 0$) is observed only in samples with $x = 0$ and $x = 0.1$ below certain temperature ($T < T_{MI}$). These samples exhibit thermal irreversibility behavior for a field-cooled (FC) and zero-field-cooled (ZFC) magnetization data in a magnetic field of 100 Oe. This is ascribed to the competition between the superexchange and double exchange interactions. The change in physical properties has been correlated to chemical parameters such as ionic radii, tolerance factor, electronegativity and variation in Mn–O–Mn angle.

PACS: 75.47.Lx; 75.47.Gk

Keywords: Manganites; Magneto-transport; Sr-substitution

1. Introduction

The manganites have generated great deal of interest because of its rich phase diagram and technological importance [1,2]. The strong correlation between magneto-transport and structural properties is responsible for most of the experimental observations in these systems. The variation in average size of the A-site cation of these perovskites ($(RR')_{2/3}M_{1/3}MnO_3$, where R and R′ are rare earth elements and M is alkaline earth element), leads to a large change (∼several orders of magnitudes) in the residual resistivity $\rho(0)$, Curie temperature T_c and the metal to insulator transition temperature, T_{MI} [3]. These changes are generally accounted due to the average size of the A-site cation, $<r_A>$, and the size mismatch at the A-site $\sigma^2(r_A)$ [4] which modifies the Mn–O–Mn bond angle and distance, and hence affect the e_g electron hopping between Mn^{3+} and Mn^{4+} states. The effect of ionic size variation is expressed through the tolerance factor defined as $t = (< r_A > + r_O)\sqrt{2}(r_B + r_O)$, where r_O and r_B are the radii of the oxygen and the B-site transition metal ions, respectively [5]. The presence of mixed valance states of Mn ion gives rise to the competing superexchange (SE) and double exchange (DE) interactions. The electronic properties of the manganites can be tailored either by substituting cations at the A- or the B-sites or by varying the oxygen content in the regular perovskite structure. The A-site ion can be substituted, for example, either by another rare earth ion or alkaline earth ion. The systematic variation of residual resistivity (ρ_0) with A-site ionic radii, in case of varied rare earth ion concentration has been well reported [6,7]. The residual resistivity increases with increasing $<r_A>$ in varied alkaline earth ion compositions which are not in agreement with the established $<r_A>$-ρ_0 phase diagram for rare earth varied manganites [6]. This suggests that

* Corresponding author. Tel.: +91 22 25767632; fax: +091 22 25723480.
E-mail address: dhirenb@iitb.ac.in (D. Bahadur).

0925-8388/$ – see front matter © 2006 Elsevier B.V. All rights reserved.
doi:10.1016/j.jallcom.2006.10.067

apart from A-site ionic radii some other parameters influence the physical properties. It appears that electronegativity difference between rare earth (RE) and alkaline earth (AE) ion also affect the transport and magnetic properties [8]. An electronegativity difference between RE and AE elements is large which leads to more ionic character with varying AE ion concentration. The ionic size of AE ions (Ba^{2+} = 1.61 Å and Sr^{2+} = 1.44 Å) is larger than that of RE ions (La^{3+} = 1.31 Å and Sm^{3+} = 1.24 Å). The substitution by larger ion at A-site leads to distortion of the lattice. The larger ion will move according to the slip system criteria, and hence the Mn–O–Mn bond angle deviates more from 180°. The slip plane is $\{1\,1\,1\}$ and slip direction is along $\langle 1\,\bar{1}\,0\rangle$ in perovskite structure. The deviation in Mn–O–Mn bond angle from 180° would obviously affect the transport and magnetic properties.

In the present study, we have undertaken a study on the series $(La_{1/3}Sm_{2/3})_{0.67}Ba_{0.33-x}Sr_xMnO_3$ for $x = 0.0, 0.1, 0.2$ and 0.33 (where the rare earth ion concentration is kept fixed and the alkaline earth ion concentration is varied), to understand the affect of chemical properties such as ionic size variation and electronegativity of alkaline earth ion on the magnetic and transport properties.

2. Experimental details

The polycrystalline $(La_{1/3}Sm_{2/3})_{0.67}Ba_{0.33-x}Sr_xMnO_3$ ($x = 0.0$, 0.1, 0.2 and 0.33) samples were synthesized by the chemical citrate-gel route using high purity La_2O_3, Sm_2O_3, $CaCO_3$, $BaCO_3$, $SrCO_3$ and Mn-acetate. The as prepared powders were calcined at 1000 °C in air for 2 h. The powders were pelletized in the form of rectangular bars and sintered at 1200 °C in air for 2 h. X-ray diffractograms of the samples were recorded using Cu Kα radiation (PW 3040/60 Philips, PANalytical). Resistivity measurements at different applied magnetic fields were made between 320 and 5 K using the standard four-probe dc method (PPMS, Quantum Design). Magnetic measurements were made using vibrating sample magnetometer (VSM, Oxford) at different fields and in the temperature range of 5–300 K.

3. Results and discussion

Fig. 1 shows X-ray diffraction patterns for the series $(La_{1/3}Sm_{2/3})_{0.67}Ba_{0.33-x}Sr_xMnO_3$ ($x = 0.0$, 0.1, 0.2 and 0.33). All the samples are single phase and crystallize in an orthorhombic structure. The cell volume decreases with decreasing A-site ionic radius. The average A-site ionic radius, $\langle r_A \rangle$ varies from 1.389 Å for $x = 0$ to 1.333 Å for $x = 0.33$ samples. The mean radius has been calculated using the coordination number 12 [9]. The tolerance factor, t, varies from 0.9883 (for $x = 0$) to 0.9680 (for $x = 0.33$). This indicates that the structure tends towards pseudo-cubic symmetry as Sr content decreases.

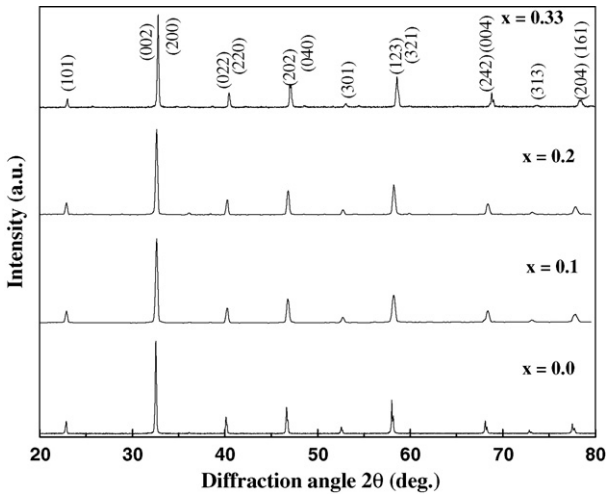

Fig. 1. X-ray diffraction patterns of the series $(La_{1/3}Sm_{2/3})_{0.67}Ba_{0.33-x}Sr_xMnO_3$ ($x = 0$, 0.1, 0.2 and 0.33).

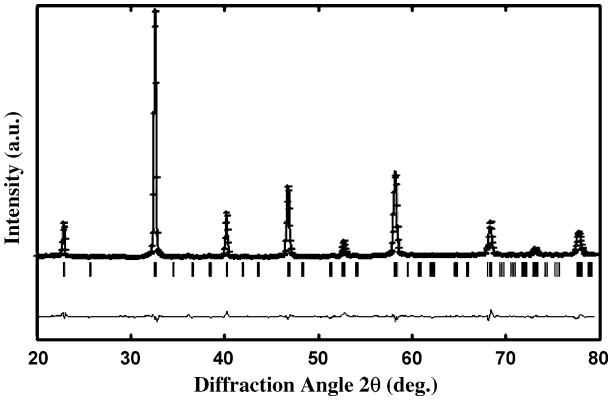

Fig. 2. Observed and fitted X-ray diffraction pattern of $(La_{1/3}Sm_{2/3})_{0.67}Ba_{0.23}Sr_{0.1}MnO_3$.

The structural parameters of all the samples were refined by the Rietveld method using the computer code FULLPROF [10]. The refinement was carried out in the space group *Pnma* (no. 62) with the following atomic positions: La/Sm/Ba/Sr: 4c(x, y, 1/4), Mn: 4b(0, 0, 1/2), O(1): 4c(x, 1/4, z) and O(2): 8d(x, y, z). A typical refined X-ray pattern with ($x = 0.1$) is shown in Fig. 2. The lattice parameters, tolerance factor, size variance ($\sigma^2(r_A) = \langle r_A^2 \rangle - \langle r_A \rangle^2$), are summarized in Table 1.

3.1. Transport

The normalized resistivity (ρ) versus temperature, (T) curves for the series $(La_{1/3}Sm_{2/3})_{0.67}Ba_{0.33-x}Sr_xMnO_3$ ($x = 0$, 0.1, 0.2

Table 1
Refined lattice parameters (using Rietveld method), tolerance factors (t), size variance $\sigma^2(r_A)$, T_c and T_{MI} for the series $(La_{1/3}Sm_{2/3})_{0.67}Ba_{0.33-x}Sr_xMnO_3$ ($x = 0$, 0.1, 0.2 and 0.33)

x	a (Å)	b (Å)	c (Å)	V (Å)^3	σ^2 (r_A) ($\times 10^{-2}$ Å^2)	t	T_c (K)	T_{MI} (K)
0.0	5.5056 (4)	7.7801 (7)	5.5022 (8)	235.68 (10)	6.08	0.9883	96	56
0.1	5.5029 (3)	7.7522 (5)	5.4859 (6)	234.02 (6)	3.83	0.9804	112	68
0.2	5.5011 (6)	7.7502 (3)	5.4851 (8)	233.85 (6)	2.09	0.9742	127	98
0.33	5.4722 (3)	7.7063 (8)	5.4599 (2)	230.25 (1)	0.59	0.9680	203	196

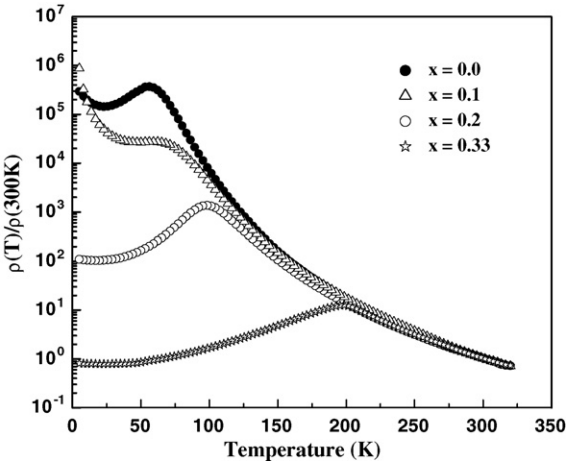

Fig. 3. Variation of normalized resistivity with temperature for the series $(La_{1/3}Sm_{2/3})_{0.67}Ba_{0.33-x}Sr_xMnO_3$ ($x = 0$, 0.1, 0.2 and 0.33).

and 0.33) are shown in Fig. 3. Metal-insulator transition temperature, T_{MI}, shifts towards higher temperatures with increasing Sr-substitution from 56 K for $x = 0$ to 196 K for $x = 0.33$. The reentrant semiconducting behavior is due to charge localization effect at low temperatures observed for compositions with $x = 0$ and 0.1.

The electronegativity of Ba (0.89) is smaller than that of Sr (0.95). The ionic characteristic of the A–O bonds increases with decreasing Sr content due to increasing electronegativity difference between A-site ion and oxygen which may lead to the charge localization behavior. The replacement by the larger ion (e.g. Ba or Sr) at A-site will lead to distortion in the lattice. The oxygen ions sitting at face centered position move towards the slip direction $\langle 1\,\bar{1}\,0\rangle$ in $\{1\,1\,1\}$ slip plane which is a higher density plane. The simplistic schematic arrangement of the ions in (1 1 1) plane is shown in Fig. 4.

The Mn–O–Mn bond angle has been estimated by using pseudo-cubic coordinates ($a/\sqrt{2}$, b/2 and $c/\sqrt{2}$). BO′ is calculated by using, $[2(r_{AE} + r_O)/\sqrt{2}]/2$, where r_{AE} is ionic radii of alkaline earth elements and r_O is the radii of oxygen ion [11]. O′T is calculated by pseudo-cubic lattice parameters where OO = O′O′.

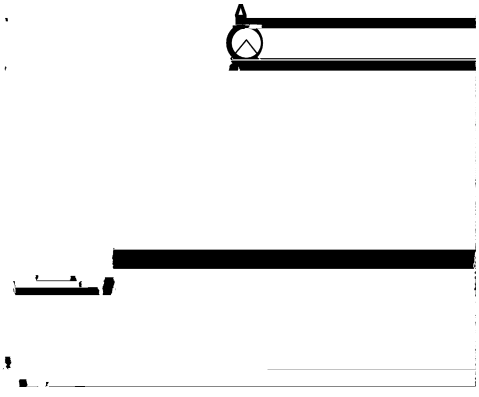

Fig. 4. A schematic diagram of (1 1 1) plane of perovskite. A-site ions are at corner positions (hollow circle), B-site ion is at center and black and hatched circles are normal oxygen and displaced oxygen ions, respectively.

The Mn–O–Mn bond angle is calculated by us using this model for $Pr_{0.7}Sr_{0.3}MnO_3$ and $Pr_{0.7}Sr_{0.1}Ca_{0.2}MnO_3$ and the values are 157.7° and 159.3°, respectively which are close to the experimental value of 159.5° and 158.3° reported by Lin [12]. The bond angle has been calculated here, for $(La_{1/3}Sm_{2/3})_{0.67}Ba_{0.33-x}Sr_xMnO_3$ ($x = 0$, 0.1, 0.2 and 0.33) using the same methodology. The Mn–O–Mn bond angle increases with increasing Sr content from 137° (for $x = 0$) to ∼158° (for $x = 0.33$). The hopping integral is defined as $t_{ij} = t_0 \cos(\theta_{ij}/2)$ where θ_{ij} is the angle between the spins on neighbouring sites. The hopping integral increases from 93% (for $x = 0$) to 98% (for $x = 0.33$) with increasing Mn–O–Mn bond angle which leads to more parallel spin arrangement. As a consequence of this, the resistivity drops with increasing Sr content.

The T_{MI} decreases with increasing size variance ($\sigma^2(r_A)$ which is strongly indicative of the presence of disorder present in the Ba containing samples. It is observed that the low size mismatch valued samples ($x = 0.2$ and 0.33) exhibit the conventional metal-insulator transition exhibited by manganites while those having higher $\sigma^2(r_A)$ show different transport behavior below T_{MI}. It could be due to the simultaneous presence of spin glass (SG) like, short-range charge order (CO) and ferromagnetic (FM) phases especially in Ba-rich samples [4]. It is shown that a magnetic and charge-order Bravais lattice exists for $A^{3+}_{1-x}B^{2+}_xMn^{3+}_{1-x}Mn^{4+}_xO_3$ for $x = n/8$ where n is an integer and the cell constant is 2a, double that of the chemical cell [13]. The charge ordered phase is more prominent with $x = 1/2$ (sharp electronic transition) rather than $x = 1/3$ where the transition is quite diffused. The increase of residual resistivity by six order from $\rho(0) = 1\ \Omega$ cm for $x = 0.33$ ($\sigma^2(r_A) = 0.59 \times 10^{-2}$ Å^2) to $\rho(0) = 10^6\ \Omega$ cm for $x = 0$ ($\sigma^2(r_A) = 6.08 \times 10^{-2}$ Å^2) samples, gives a strong support to the effect of local atomic disorder on the carriers scattering [14]. This local atomic disorder may cause the emergence of SG-like phase over FM phase which presumably increases with more atomic disorder. The large size variance could also lead to the canting of spins which in turn lead to localization at low temperatures and this is reflected in the $\rho(T)$ plots of the samples with $x = 0$ and 0.1 (Fig. 3). The possibility of electronic phase separation is also consistent with magnetization results as discussed later.

3.2. Magnetoresistance

Fig. 5 shows the magnetoresistance behavior of the series $(La_{1/3}Sm_{2/3})_{0.67}Ba_{0.33-x}Sr_xMnO_3$ ($x = 0$, 0.1, 0.2 and 0.33) in 80 kOe applied magnetic field. In the presence of an external field, the resistivity decreases significantly. The decrement in resistivity suggests that the external magnetic field facilitates the hopping of e_g electrons between neighbouring Mn ions, which agrees with the DE model [15,16]. The magnetoresistance (MR) is defined as

$$\%MR = 100 \times \frac{[\rho(H, T) - \rho(0, T)]}{[\rho(0, T)]}, \quad (1)$$

where $\rho(H,T)$ and $\rho(0,T)$ are the resistivities at a temperature T, in an applied magnetic field H and in zero applied magnetic field,

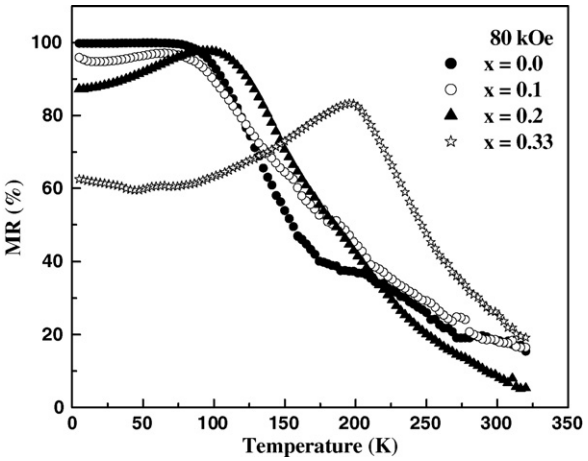

Fig. 5. Variation of %MR with temperature for series $(La_{1/3}Sm_{2/3})_{0.67}Ba_{0.33-x}Sr_xMnO_3$ ($x = 0$, 0.1, 0.2 and 0.33) in 80 kOe field.

respectively. The maximum value of MR (~99.9% at 80 kOe) is observed in Ba rich samples as compared to the sample with $x = 0.33$ (~85%). The manganese ions are ferromagnetically ordered below T_c; therefore, within a single magnetic domain, the e_g electron transfer between Mn^{3+} and Mn^{4+} ions is easy. The pairs of Mn^{3+} and Mn^{4+} spins, which may not be parallel in the vicinity of domain wall boundaries, will act as a hindrance for electron transport. The domain wall rotation starts above a field of 10 kOe as indicated from the M versus H plots. Therefore, magnetic domains tend to align along the field direction in the presence of sufficiently strong (>10 kOe) magnetic field. As a result, hopping of electrons becomes easier across the domain wall boundaries and the resistivity decreases, which in turn leads to a significant MR at low temperatures. A weakly temperature dependent high MR is observed below 100 K, which may be ascribed to a combined effect from canting of spins [17] and melting of short range CO phases into FM phase in an applied magnetic field of 80 kOe [4]. These effects also lead to high values of MR particularly at lower temperatures. Therefore, Ba-rich samples show the highest and temperature independent MR at low temperatures, which could be due to progressive alignment of canted spin or transformation of antiferromagnetic (SG-like or CO) phase into a ferromagnetic ordered phase at 80 kOe magnetic fields as a function of lowering the temperature. The highest value of MR (~99.9% at 80 kOe and below 100 K) is seen for sample with $x = 0$.

3.3. Magnetization

The variation of magnetization with temperature in both the zero field cooled (ZFC) and field cooled (FC) conditions for the series $(La_{1/3}Sm_{2/3})_{0.67}Ba_{0.33-x}Sr_xMnO_3$ ($x = 0$, 0.1, 0.2 and 0.33) measured at 100 and 1000 Oe fields are shown in Figs. 6 and 7, respectively. Thermal irreversibility behavior in zero field cooled (ZFC) and field cooled (FC) magnetization is observed in all the cases and is more obvious if the measurements are done in a field of 100 Oe. The extent of this thermal irreversibility increases from $x = 0$ to $x = 0.2$ and then drops

Fig. 6. Plot of magnetization during ZFC and FC cycles as a function of temperature for the series $(La_{1/3}Sm_{2/3})_{0.67}Ba_{0.33-x}Sr_xMnO_3$ ($x = 0$, 0.1, 0.2 and 0.33) measured at 100 Oe.

in case of the sample with $x = 0.33$. A small anomaly around 50 K is observed in all cases. This anomaly has been reported in the substituted manganites and has been explained on the basis of microscopic magnetic inhomogenities arising from the variable Mn oxidation states [18–20]. These inhomogenities lead to the electronic phase separation at nano-scale length. The temperature at which the ZFC and FC plots bifurcate is known as freezing temperature and designated as T_f. The shift of T_f to lower temperatures with increasing fields has been attributed to increasing antiferromagnetic (AFM) interaction, which is a characteristic of spin/cluster glass like system [21]. The paramagnetic (PM) to ferromagnetic (FM) transition is observed in all systems. This magnetic transition becomes broader with increasing fields.

The T_c increases with Sr content presumably due to increasing overlap integral. The difference between T_c and T_{MI} decreases with increasing Sr content which indicates that the long range ferromagnetic ordering vanishes as the concentration of Sr decreases due to the larger size variance. The inset of Fig. 7 shows the M(T) variation in FC mode for the sample with $x = 0.33$ measured at 5 kOe.

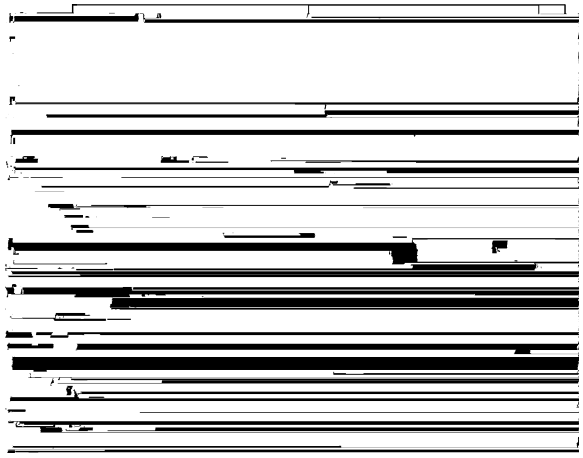

Fig. 7. The magnetization variation with temperature in 1 kOe fields for the series $(La_{1/3}Sm_{2/3})_{0.67}Ba_{0.33-x}Sr_xMnO_3$ ($x = 0$, 0.1, 0.2 and 0.33). Inset shows the M–T plot for $x = 0.33$ in 5 kOe field.

We conclude that the frustration due to the competing FM and AFM causes the phase separation in these systems. The frustration is more pronounced in Ba-rich samples which are reflected from transport as well magnetic studies. Hence, the tendency of phase separation increases with increasing Ba-content.

The overall magnetic behavior may be explained by de Gennes [16] model according to which the Curie temperature for a ferromagnetic spin arrangement in $La_{1-x}Ca_xMnO_3$ is given by

$$k_B T_c = \frac{2}{3}\left[z_a|J^a| - z_b|J^b| - z_c|J^c|\right] S^2 + \frac{2xz\varepsilon_p}{5} \quad (2)$$

where z_i ($i = a$, b, c) are the numbers of nearest neighbours along the a-, b- and c-directions, z is the total number of nearest neighbours and J^i is the effective exchange integral in the i- direction and ε_p is the gain in energy due to hopping. The spin arrangement for $\varepsilon_p = 250$ K is that of a collinear ferromagnet for $x > 0.26$ [13]. The first term in the Eq. (2) comes from the antiferromagnetic and the second term is due to the ferromagnetic interaction, namely double exchange. The value of x is 0.33, which is fixed in our case. Taking $J^a = 1.61$ meV, $J^b = J^c = 0.62$ meV, $\varepsilon_p = 250$ K, $z = 6$, the T_c is 215 K for $(La_{1/3}Sm_{2/3})_{0.67}Sr_{0.33}MnO_3$ which is close to the experimental value of 203 K. The local atomic disorder increases with decreasing Sr content as a result of which the ferromagnetic interactions becomes weaker as compared to antiferromagnetic interaction. The drop in the magnetization could be explained by the strong antiferromagnetic interaction below a particular temperature.

Fig. 8 shows the isothermal magnetization field plots of the series $(La_{1/3}Sm_{2/3})_{0.67}Ba_{0.33-x}Sr_xMnO_3$ ($x = 0$, 0.1, 0.2 and 0.33). All the samples exhibit near saturation in magnetization except the $x = 0.33$ sample which is saturated. As expected, there is no significant change in magnetization value at high fields among these samples. The Ba-rich ($x = 0.0$ and 0.1) samples show the non-saturating M–H behavior even in 40 kOe fields as shown in the inset of Fig. 8. This non-saturating M–H behavior may be attributed to canting of spins with decreasing Sr content. The possibility of spin canting is more significant in Ba-rich samples due to atomic disorder and competing antiferromagnetic (SE) and ferromagnetic (DE) interactions which leads to frustration in these systems [22].

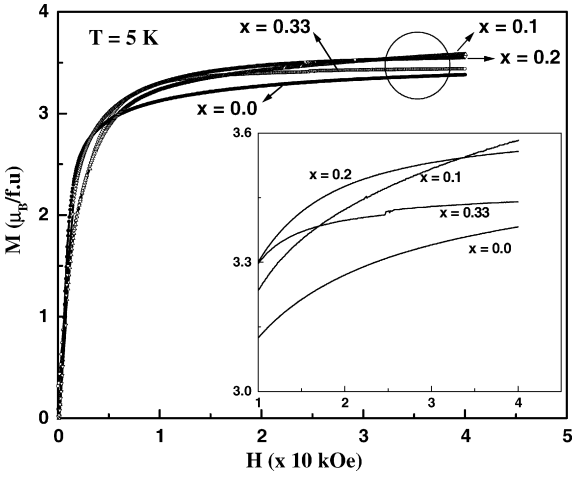

Fig. 8. Isothermal magnetization at 5 K for the series $(La_{1/3}Sm_{2/3})_{0.67}Ba_{0.33-x}Sr_xMnO_3$ ($x = 0$, 0.1, 0.2 and 0.33). The enlarge view of M–H plots is shown in inset.

4. Conclusions

The effect of Sr substitution on the transport and magnetic properties of $(La_{1/3}Sm_{2/3})_{0.67}Ba_{0.33-x}Sr_xMnO_3$ ($x = 0$, 0.1, 0.2 and 0.33) compounds has been studied. All the compounds crystallize in the orthorhombic crystal structure. The T_{MI} shifts to higher temperature and the reentrant semiconducting behavior smears out with increasing Sr-content as the suppression of the charge localization occurs due to decreasing size variance or partially due to electronegativity difference between rare earth and alkaline earth ions. The transport properties could be understood by the Mn–O–Mn bond angle variation with simplistic approach. A weakly temperature independent MR can be accounted due to transformation of AFM (SG-like/short range CO) into FM phase. Bifurcation behavior in the magnetization versus temperature due to presence of frustration is observed in ZFC and FC magnetization plots in all the cases. The magnetic properties may be understood by de Gennes approach of competing superexchange and double exchange interactions. The non-saturating M–H behavior is indicative of frustration in the Ba-rich samples which also supports the above approach. The overall magnetic and transport properties could be attributed to the competing AFM and FM interactions.

Acknowledgement

The author SA and DB are thankful to the Department of Science and Technology, India for financial support.

References

[1] J. Heremans, J. Phys. D: Appl. Phys. 26 (1993) 1149.
[2] S. Jin, M. McCormack, T.H. Tiefel, R. Ramesh, J. Appl. Phys. 76 (1994) 6929.
[3] T.V. Ramakrishnan, in: C.N.R. Rao, B. Raveau (Eds.), Colossal Magnetoresistance, Charge Ordering and Related properties of Manganese Oxides, World Scientific, Singapore, 1998, pp. 325–345.
[4] Y. Tomioka, Y. Tokura, Phys. Rev. B 70 (2004) 014432.
[5] J.P. Attfield, Cryst. Eng. 5 (2002) 427.
[6] J.L. Garcia-Munoz, J. Fontcuberta, B. Martinez, A. Seffar, S. Pinol, X. Obradors, Phys. Rev. B 55 (1997) R668.
[7] L. Sudheendra, C.N.R. Rao, J. Phys. Condens. Matter 15 (2003) 3029.
[8] Z.C. Xia, B. Dong, G. Liu, D.W. Liu, L. Chen, C.H. Fang, L. Liu, S. Liu, C.Q. Tang, S.L. Yuan, Phys. Stat. Sol. (a) 202 (2005) 113.
[9] R.D. Shannon, Acta Crystallogr. A 32 (1976) 751.
[10] J. Rodrıguez-Carvajal, 2001. *FULLPROF* version 2001. Laboratoire L'eon Brillouin (CEA-CNRS)CEA/Saclay, 91191 Gif sur Yvette Cedex, France.
[11] C. Kittel, Introduction to Solid State Physics, 5th ed., Wiley Eastern Ltd., 1976.
[12] J.G. Lin, J. Phys. Chem. Solids 62 (2001) 1881.
[13] C.M. Srivastava, J. Phys. Condens. Matter 11 (1999) 4539.
[14] A. Maignan, C. Martin, G. Van Tendeloo, M. Hervieu, B. Raveau, Phys. Rev. B 60 (1999) 15214.
[15] C. Zener, Phys. Rev. 82 (1951) 403.

[16] P.G. de Gennes, Phys. Rev. 118 (1960) 141.
[17] D. Das, A. Saha, S.E. Russek, R. Raj, D. Bahadur, J. Appl. Phys. 93 (2003) 8301.
[18] H.L. Ju, H. Sohn, J. Magn. Magn. Mater. 167 (1997) 200.
[19] D. Bahadur, M. Yewondwossen, Z. Koziol, M. Foldeaki, R.A. Dunlap, J. Phys. Condens. Mater. 8 (1996) 5235.
[20] Saket Asthana, D. Bahadur, A.K. Nigam, S.K. Malik, J. Appl. Phys. 97 (2005) 10H711.
[21] C. Mitra, P. Raychaudhari, S.K. Dhar, A.K. Nigam, R. Pinto, S.M. Pattalwar, J. Magn. Magn. Mater. 192 (1999) 130.
[22] D. Saket Asthana, A.K. Bahadur, S. Nigam, K. Malik, J. Phys. Condens. Mater. 16 (2004) 5297.